Quantitative Analysis of Localized Surface Plasmons Based on Molecular Probing

Claire Deeb,[†] Renaud Bachelot,[†,*] Jérôme Plain,[†] Anne-Laure Baudrion,[†] Safi Jradi,[†] Alexandre Bouhelier,[‡] Olivier Soppera,[§] Prashant K. Jain,[∥] Libai Huang,[⊥] Carole Ecoffet,[§] Lavinia Balan,[§] and Pascal Royer[†]

[†]Laboratoire de Nanotechnologie et d'Instrumentation Optique LNIO-ICD CNRS-UMR 6279, Université de Technologie de Troyes, Troyes, France, [‡]Laboratoire Interdisciplinaire Carnot de Bourgogne CNRS-UMR 5209, Université de Bourgogne, Dijon, France, [§]Institut de Science des Matériaux de Mulhouse (IS2M-CNRS LCR 7228), Université de Haute-Alsace, Mulhouse, France, [∥]Miller Institute for Basic Research in Science and Department of Chemistry, University of California, Berkeley, California 94720, and [⊥]Radiation Laboratory, University of Notre Dame, Notre Dame, Indiana 46556

ABSTRACT We report on the quantitative characterization of the plasmonic optical near-field of a single silver nanoparticle. Our approach relies on nanoscale molecular molding of the confined electromagnetic field by photoactivated molecules. We were able to directly image the dipolar profile of the near-field distribution with a resolution better than 10 nm and to quantify the near-field depth and its enhancement factor. A single nanoparticle spectral signature was also assessed. This quantitative characterization constitutes a prerequisite for developing nanophotonic applications.

KEYWORDS: near-field optics · molecular probes · localized surface plasmon · quantitative analysis · nanoscale photopolymerization

Optical properties of localized surface plasmons (LSP) supported by metal nanostructures have given rise to many efforts and studies over the past decade.[1−5] This important branch of nanophotonics envisions many challenges and applications including solar energy harvesting,[6−8] optical manipulation,[9] efficient light generation,[10−12] local heating,[13] photothermal tumor ablation,[14−16] nanopatterning for data storage,[17,18] and nanoscale biosensing.[19,20] A detailed understanding of the near-field response of engineered plasmonic nanostructures is therefore essential for controlling and optimizing a desired outcome along the line of the applications listed above. Determining a simple method for an accurate nanometer scale imaging of confined optical fields with quantitative measurements still constitutes an open challenge.

Several efforts, namely, proximal probe methodologies[21,22] and electron microscopy,[23−25] have been made to better understand the near-field response of metal nanoparticles and their field distribution. While these methods constitute indirect and qualitative approaches of characterization, we report, in this paper, a quantitative analysis of LSP of silver metal nanoparticles using a molecular probe. Our approach relies on nanoscale molecular molding of the confined electromagnetic field by a photoactivated polymer. The particular advantages of this method are discussed throughout the paper. On the basis of our technique, we were able to directly image the dipolar profile of the near-field distribution with a resolution better than 10 nm and to quantify the near-field depth and its enhancement factor. We were also able to measure the spectral signature of the LSP resonance directly in the near-field. These results demonstrate a quantitative characterization, down to the nanometer level, of the confined evanescent optical fields that are prerequisites for developing photonic applications. To the best of our knowledge, this is the first time quantitative parameters related to localized surface plasmons have been extracted. A comparison between the measured parameters and finite-difference time-domain (FDTD) calculations support the validity of this quantification.

Description of the Approach. Our experimental approach, as schemed in Figure 1, is based on nanoscale photopolymerization triggered by the locally enhanced optical near-field of chemically synthesized silver nanoparticles (AgNPs).[26] AgNPs are anchored on a silane-functionalized glass coverslip by a dip-coating procedure (Figure 1a). The aminosilane functionalization guarantees a firm adhesion of the nanoparticles on the glass coverslip despite the various stages of rinsing.[27] To selectively address single nanoparticles of well-defined geometry, the decorated glass substrate is placed

*Address correspondence to renaud.bachelot@utt.fr.

Received for review April 20, 2010 and accepted July 27, 2010.

Published online August 5, 2010. 10.1021/nn101017b

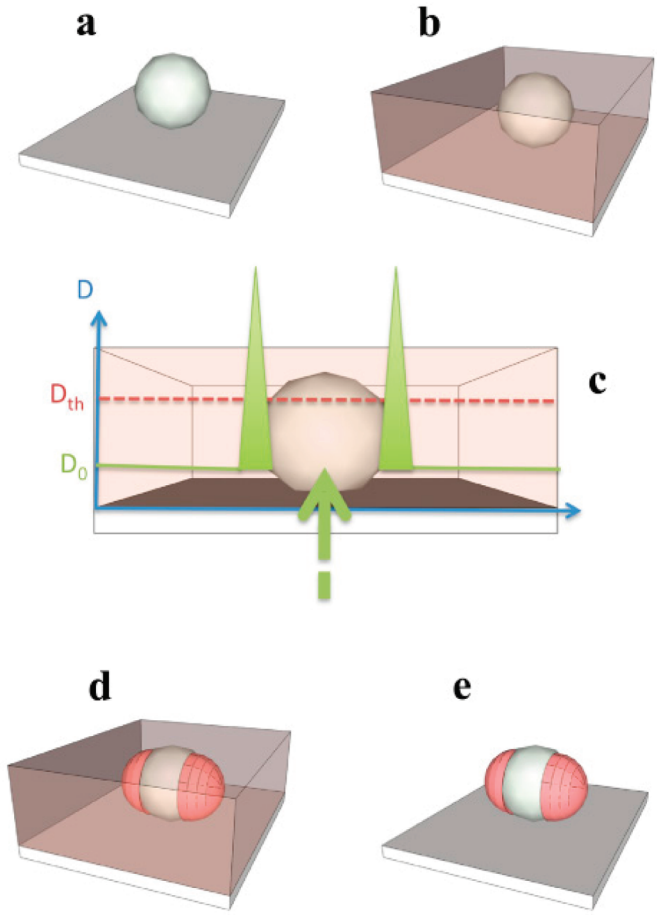

Figure 1. Scheme of the approach. (a) AgNP deposited on a functionalized glass substrate. (b) Deposition of the photopolymerizable formulation. (c,d) Plasmon-enhanced near-field photopolymerization of PPF leading to two wings corresponding to the dipolar LSP resonance. (e) Resulting hybrid nanoparticle revealed by the rinsing procedure.

on an inverted optical microscope coupled to an atomic force microscope (AFM). The nanoparticles are homogeneously covered by synthesized free radical photopolymerizable formulation (PPF) possessing high-resolution visible-light sensitivity (Figure 1b) and characterized by a threshold dose that must be overcome to induce the polymerization process. A controlled volume of PPF is deposited onto AgNPs using a pipet. A drop of 4 cm diameter, corresponding to a volume of 40 μL, was consistently obtained.

The polymerization is activated by laser irradiation with wavelengths overlapping both the PPF absorption spectrum and the AgNP plasmon resonance. The optical exposure is performed under normal incidence with a 1 cm wide linearly polarized laser beam from an Ar:Kr laser source. The exposure dose (D_0) is chosen to be smaller than the threshold dose, D_{th}, below which no polymerization can occur (Figure 1c). This threshold value is systematically quantified by far-field prestudies.[26] Therefore, photopolymerization is not expected to occur in the absence of AgNPs. Due to the field enhancement at the plasmon resonance (Figure 1c), the effective dose near the metallic nanoparticles can be greater than the threshold D_{th} to initiate the chain reaction leading to polymerization (Figure 1d). After irradiation, the obtained polymer nanoparts are revealed by removal of any monomer material that is not reticulated, by rinsing with ethanol and isopropanol (Figure 1e) and characterized by AFM using intermittent-contact mode. It should be stressed that AFM characterization before and after the exposure is performed for the same preselected individual AgNP. The coupled AFM-inverted optical microscope actually allows us to address single labeled particles and to retrieve them after the rinsing procedure. The size of the polymer wings attached to AgNPs is related to the strength and the depth of the optical near-field, which allows us to quantitatively map the plasmon response unlike few previous reports that have demonstrated plasmon-enhanced photopolymerization. In particular, Ecoffet and co-workers produced for the first time polymer nanoparts by using simple Fresnel evanescent waves generated by total internal reflection.[28] In this experiment, nanometer resolution was achieved but only along the direction perpendicular to the substrate. Wurtz *et al.* showed that the lightning rod effect at the extremity of a metal tip under laser illumination could lead to local polymerization.[29] Srituravanich and co-workers demonstrated 90 nm resolution in plasmon-based optical lithography on negative-tone photopolymer with the use of an array of nanoapertures on a metal film.[30] Sundaramurthy *et al.* qualitatively evidenced the presence of locally enhanced field in the gap of a metal bowtie antenna.[31] Ibn el Ahrach *et al.* introduced a new hybrid polymer/metal nanostructure produced by plasmon-based photopolymerization.[26] More recently, Ueno and co-workers demonstrated sub-100 nm resolution photopolymerization at the gap separating two gold nanoblocks.[32]

In all of these works, the main motivation was either to produce nanostructures through plasmon-based lithography or to perform a qualitative observation of plasmonic fields (proof of presence of hot spots, evidence for excitation of electromagnetic singularities, *etc.*). Quantification of the plasmon near-field was neither achievable nor performed. Here, a full parameter study is carried out, and quantitative parameter values related to localized surface plasmons are measured. In particular, the knowledge of the plasmon field enhancement factor still constitutes a challenge. At best, a wide range of enhancement factor values have been reported in the literature based on numerical calculation and indirect measurements. As discussed in the previous sections, our approach provides realistic values of these enhancement factors by relying on a well-referenced and well-characterized system, that is, the free radical photopolymerizable formulation.

As a first result, Figure 2 demonstrates the ability to directly visualize the optical near-field with the approach described above.

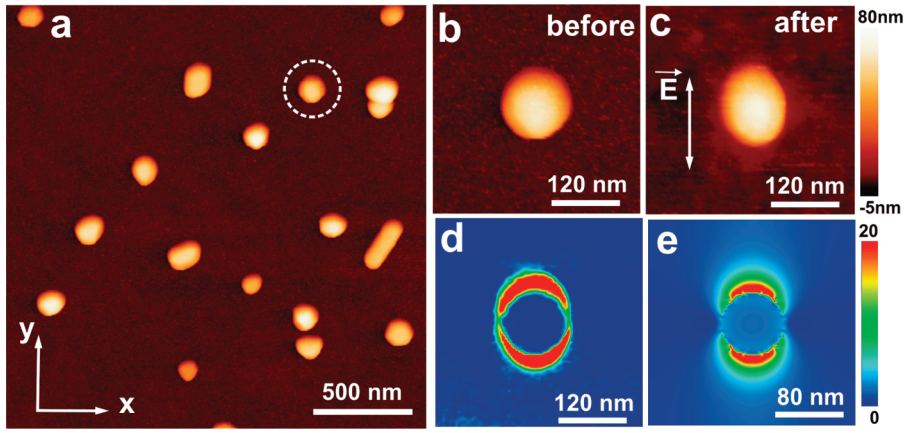

Figure 2. Near-field photopolymerization based on the resonant excitation of the dipolar plasmon mode of AgNPs. (a) Topographic AFM image of AgNPs before the procedure. (b) Magnified image of a. (c) Magnified topographic image of AgNPs after the procedure. (d) Differential image of panels c and b. (e) Near-field intensity as calculated by FDTD.

Figure 2a shows a topographic image of AgNPs deposited on the functionalized glass before exposure. A single isolated particle was chosen (circle) to demonstrate our ability to map the field down to sub-10 nm resolution. Due to tip convolution, its apparent diameter is 110 nm, while its actual diameter is 60 nm as deduced from the height of a cross section acquired through the center of the AgNP. Since the colloidal particles used are spherical, the height acquired from a section sketched along the metal structures represents their diameter. Throughout our analysis, similar sized and nearly spherical particles were considered. A magnified image of the selected particle is displayed in Figure 2b.

After PPF coverage, the AgNPs were illuminated with a *y*-oriented linearly polarized laser beam with $\lambda = 514$ nm. The exposure dose D_0 was set to 63% of D_{th}. The threshold conditions of the PPF used here have been determined to be incident power $P = 2$ mW/cm^2 with an irradiation time $t = 3.5$ s, implying a threshold dose D_{th} of 7 mJ/cm^2. We kept the incident laser power constant at 2 mW/cm^2, while varying the irradiation time across our experiments. As a typical example, in order to set D_0 to 63% of D_{th}, we set $P = 2$ mW/cm^2 and $t = 2.2$ s.

Figure 2c shows a topographic image of the selected particle after rinsing. The particle exhibits an elongation along the *y*-direction that results from the photopolymerization initiated by the enhanced local field. It should be highlighted that Figure 2b,c was obtained for the same metal nanoparticle with the same tip under the same scanning conditions.

In order to highlight the localized photopolymerization, we subtract Figure 2b from Figure 2c, resulting in Figure 2d. Such a differential image accurately depicts the spatial distribution of the polymerization resulting from the reticulation process, while circumventing the apparent increase of the polymer depth due to convolution with the AFM tip. Figure 2d clearly reveals two polymer wings oriented along the incident polarization direction. To elucidate the origin of wings, we numerically map in Figure 2e the electric field intensity distribution around an isolated AgNP using finite-difference time-domain (FDTD) simulations. The field distribution is calculated for a spherical 60 nm AgNP embedded in a medium of refractive index 1.485, matching that of the PPF. The calculation shows a two-lobe pattern characteristic of a dipolar near-field distribution. The similarity between Figure 2d and Figure 2e implies that the enhanced localized near-field is responsible for the nanoscale photopolymerization.

RESULTS AND DISCUSSION

We studied the dependence of the size of polymer wings on the exposure dose (Figure 3). Figure 3a shows the height difference of a typical AgNP obtained by subtracting the topographic profile along the *y*-axis before from that after the reticulation procedure (without laser exposure). Figure 3b shows the differential profile along the *y*-axis obtained by subtracting the topographical profile before polymerization from that after polymerization using a dose of $0.75D_{th}$. Two peaks with a 25 nm height and 20 nm full width at half-maximum (fwhm) are obtained. The differential profile of Figure 3c illustrates the situation for a much lower incident dose of $0.05D_{th}$, where the fwhm of the polymer wings is much narrower (<10 nm). We explain this dependence as follows. For an exposure dose of $0.75D_{th}$, photopolymerization can occur at any location where the field enhancement factor exceeds $D_{th}/D_0 = 1.33$; while for an exposure dose of $0.05D_{th}$, only locations with an enhancement factor higher than $D_{th}/D_0 = 20$ will support photopolymerization. At $0.05D_{th}$, we thus map the regions with an enhancement exceeding 20, with a resolution better than 10 nm (*i.e.*, $\sim\lambda/50$).

To the best of our knowledge, this is the first time a sub-10 nm resolution photopolymerization is being demonstrated in the visible region, allowing, in turn, a sub-10 nm optical resolution characterization of plasmonic structures. Our unprecedented resolution is due

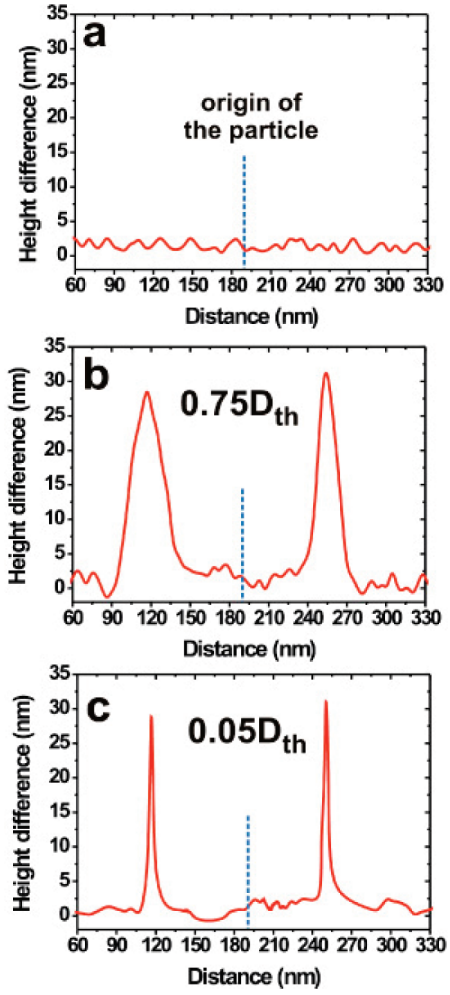

Figure 3. Molding the LSP near-field intensity by the process of photopolymerization. (a) Reference profile: height difference of a AgNP taken along the *y*-axis before and after the procedure (without laser exposure). Differential profile along the *y*-axis for (b) 0.75D_{th} and (c) 0.05D_{th}.

to the use of the free radical formulation designed *in house* and optimized for molecular-level resolution,[28] rather than commercial SU-8 resin that has been optimized only for UV-blue far-field lithography.[32]

It should be noted that, although image differentiation allows one to evaluate the actual width of the polymer wings, the apparent distance between the two wings is increased by AFM tip convolution. It must be pointed out that the usage of the same AFM tip before and after the exposure may cause an enlargement in its size, leading to an artificial broadening in the AFM image. In order to make sure that such artifact does not affect our results, we calculated differential profiles along the direction perpendicular to the incident field (along *x*-axis) where no field enhancement is expected. Figure 4 shows this differential profile obtained by subtracting the topographical profile before polymerization from that after polymerization using a dose of 0.75D_{th}. The flat differential profile when compared to Figure 3b,c clearly demonstrates that the AgNP has the same apparent size and geometry along the *x*-direction before and after the procedure. This implies that the AFM tip had almost the same characteristics while scanning the two images, made which is possible by our ability to retrieve our region of interest rapidly without compromising the tip quality.

We show in Figure 5 additional evidence that the dipolar profile of the AgNP LSP is solely responsible for the observed nanoscale photopolymerization and that AgNP elongation is not due to a sample drift during the AFM scan.

Figure 5a shows a topographic AFM image of a AgNP with high in-plane symmetry before the laser exposure. Figure 5b illustrates the AFM image of the same particle after being exposed to the laser beam with polarization along the vertical direction. Figure 5c shows an AFM image of the same nanoparticle after rotating the sample by 45°. It should be noted that the fast scan direction is always kept along the *x*-axis for all three panels of Figure 5. The selected AgNP exhibits an elongation (Figure 5b) in the same direction as the laser polarization shown by the red arrow. When the sample is rotated by 45° (Figure 5c), the elongation of the particle persists in the direction of the incident field, demonstrating that the imaged elongation of the AgNP is not an artifact due to sample drift but it is purely due to nanoscale polymerization triggered by the LSP of the AgNP.

We performed systematic quantitative studies of the size of the polymer wings as a function of the dose.

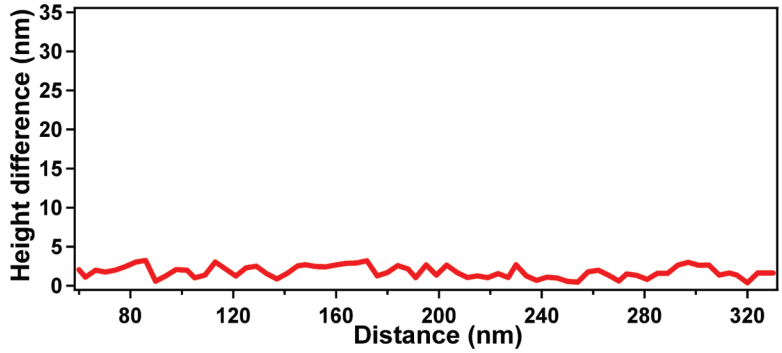

Figure 4. Height difference of a AgNP taken along the *x*-axis before and after the polymerization for an incident dose of 0.75D_{th}.

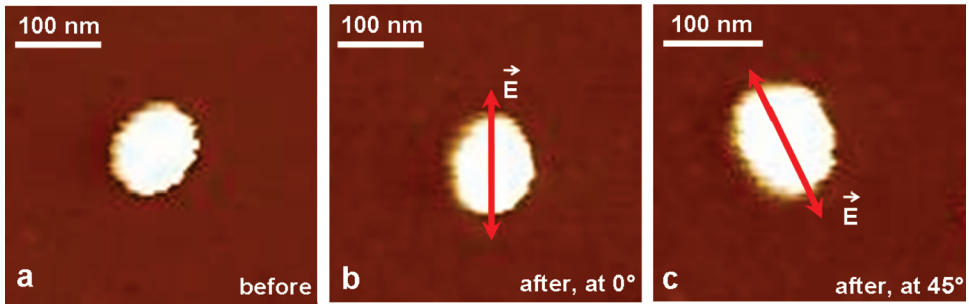

Figure 5. (a) AFM image of a selected nanoparticle before irradiation. (b) AFM image after irradiation where the fast scan direction is along the *x*-axis and perpendicular to the incident field polarization direction. (c) AFM image for the same particle with fast scan direction along the *x*-axis direction and the same irradiated sample rotated by 45°.

Figure 6a shows the averaged full width w (red squares) of the polymer that was reticulated as a function of d, the normalized incident dose D_0/D_{th}. Each point corresponds to an average of three experiments made on three identical particles exposed with the same dose. The graph demonstrates a monotonic increase of w with d.

This result can be understood by considering the near-exponential decay of the near-field of the excited nanoparticle. The local dose D provided by the metallic nanoparticle in the y-direction can be expressed as

$$D = F_{max} D_0 \exp(-\alpha y) \quad (1)$$

where F_{max} is the maximum (or surface) intensity enhancement factor related to the LSP resonance, α is the rate of field intensity decay, and y is the distance from the surface of the metallic nanoparticle in the y-direction; α^{-1} can be viewed as the spatial extension of the near-field intensity. We consider here the y-direction because along this direction the incident field is perpendicular to the metal/dielectric interface, allowing surface charges to be excited.[33] Second, α is an average of the continuous spectrum of decay lengths (each of them being associated with lateral wave vectors) of the angular spectrum generated by the AgNP diffraction.[34]

As discussed in a previous section, photopolymerization occurs when $D > D_{th}$. By applying this condition to eq 1, one can obtain

$$\exp(-\alpha y) \geq \frac{D_{th}}{F_{max} \times D_0} \quad (2)$$

By reducing eq 2, we get the locations where the photopolymerization can occur as given by

$$y < y_{max} = -\alpha^{-1} \ln\left(\frac{D_{th}}{F_{max} \times D_0}\right) \quad (3)$$

Replacing D_0/D_{th} by the normalized dose d, we get the value of y_{max} as

$$y_{max} = \alpha^{-1} \ln(F_{max} \times d) \quad (4)$$

where y_{max} corresponds to the maximum distance away from the AgNP at which the effective dose (incident dose amplified by the enhancement factor of AgNP) overcomes the threshold dose. Since up to this distance y_{max} the threshold dose is exceeded, the polymerization is observed. The width w detected by AFM, thus, corresponds to this distance y_{max}, allowing us to express the measured width w as $w = \alpha^{-1} \ln(F_{max} d)$. By fitting our experimental data with a logarithmic function (Figure 6a, solid line), we obtain F_{max} and α^{-1} as 39 and 11 nm, respectively. From eq 4 or the data from Figure 6a, we can extract the distance dependence of the local field enhancement factor (*i.e.*, $1/d = F_{max} \exp(-\alpha w)$).

Figure 6b plots $1/d$ as a function of w. The data follow a single-exponential decay reflecting the near-exponential decay of the plasmon near-field. The experimental data are also in good agreement with FDTD simulations (black curve). The latter was fitted with an exponential function (dashed green curve) with values of F and α^{-1} of 34 and 10 nm, respectively, which are in close agreement with the experimentally measured parameters. The excellent agreement between the experi-

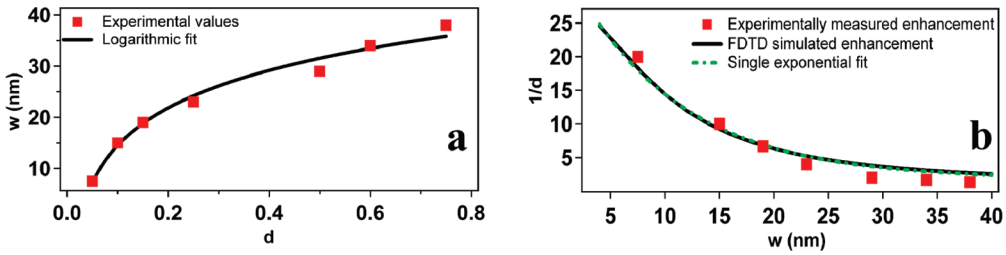

Figure 6. Quantification of the physical parameters related to localized surface plasmons. (a) Effect of the incident dose on the photopolymerization width of the polymer: experimental value (red squares) and fitting function $y = 11\ln(39 \times d)$. (b) Experimental values (red points) of the local field enhancement factor of AgNPs plotted as a function of the polymer width measured by AFM. Black line corresponds to the FDTD-simulated enhancement, and green line is a single-exponential fit.

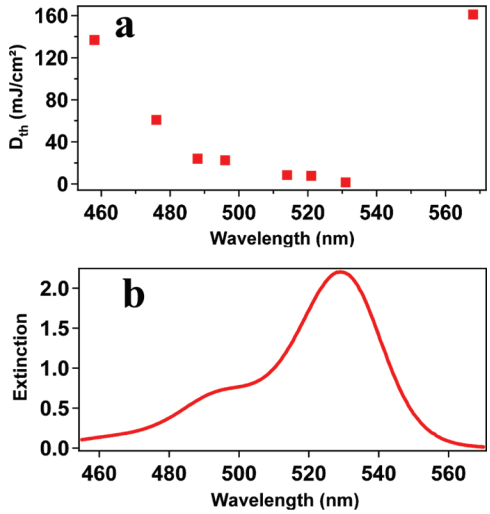

Figure 7. Spectral response of the photochemical system characterized in the far-field. (a) Variation of D_{th} as a function of the incident wavelength. (b) Absorption spectrum of the Eosin-Y dye in the photochemical system.

mental data and the FDTD simulations strongly supports that our approach is able to profile the optical near-field of a single metallic nanoparticle with nanometer precision. Our results further indicate that the near-field depth α^{-1} is ~0.2 times the nanoparticle diameter, which is consistent with the distance decay observed for near-field coupling in particle pairs.[35] Our direct mapping of the plasmonic field, thus, confirms the near-field distance dependence proposed on the basis of indirect far-field spectra.[35] To the best of our knowledge, this near-field depth value constitutes the first experimental measurement achieved directly in the near-field.

It should be stressed that the present approach of plasmon near-field characterization is direct. Near-field scanning probe optical microscopies (NSOM) have allowed extraction of immense optical information about metal nanostructures over the past two decades.[21,22] However, NSOM is not a direct method and constitutes an inverse problem in the sense that, in NSOM, the near-field interaction between tip and sample leads to propagating waves that are integrated and detected in the far-field (Huygens Fresnel Principle). The precise control of the position of the tip along with the scan allows for subwavelength near-field imaging. The achieved resolution depends on many parameters including the nature of the interaction, the tip-to-sample distance, and the tip size. What is actually measured in NSOM is the far-field of a system resulting from the subtle "controlled" coupling between tip and sample. A primary issue with NSOM is that the nature of the signal depends very much on the tip quality as well as its surrounding environment. As a specific example, the signal from an apertureless NSOM can be proportional to either the intensity or to the complex field depending on the presence of surrounding scatterers acting as reference fields of an interferometric system.[36] An alternative way is to use single scatterers (*e.g.*, molecules, quantum dots, *etc.*) to characterize the near-field *via* fluorescence emission.[37] However, in these methods, the fluorescence signal reports the competition between tip-induced near-field enhancement and quenching (energy transfer).

Due to the dispersive nature of the plasmon response, F_{max} is a function of λ, and therefore, the local photopolymerization should reflect the LSP spectral dependence. Unlike the traditional approach of far-field spectroscopy,[38] our approach provides for the first time the opportunity to investigate this dispersive relationship directly in the near-field. To illustrate this capability, we used eight available wavelengths of the Ar:Kr source. The spectral response of the photochemical system (*i.e.*, the function $D_{th}(\lambda)$) is characterized by far-field spectral investigation of D_{th}. Figure 7a shows the measured D_{th} as a function of the incident wavelength. A clear minimum is observed at $\lambda = 530$ nm. This minimum corresponds to the maximum of the absorption spectrum (530 nm) of the Eosin-Y dye used as a photosensitizer (Figure 7b). The knowledge of the D_{th} for each λ allows us to set the normalized dose d at a constant value.

Figure 8a shows the polymer thickness w for isolated AgNPs as a function of wavelength for constant $d = 0.75$. Here we neglect the influence of the photochemical effects (in particular, the diffusion of oxygen and dye) by considering them to be constant parameters. Since w is related to F_{max} as shown earlier, the spectrum in Figure 8a reflects the near-field spectral response of the AgNP. The spectrum shows a clear resonance attributable to the spectral signature of the underlying LSP mode, with a maximum at 494 nm as per a Gaussian fit (black curve). Our characterization ap-

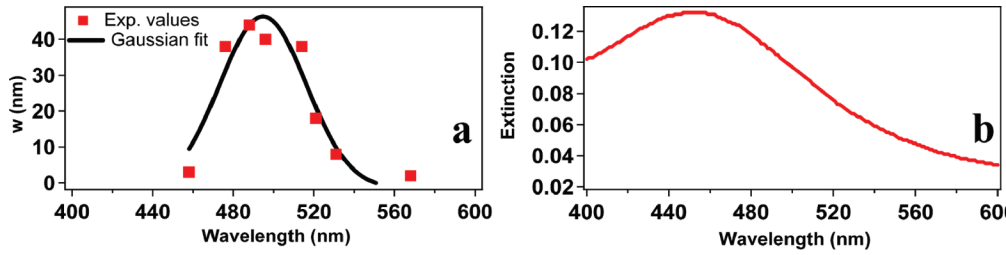

Figure 8. Near-field spectral signature of the LSP resonance of isolated AgNPs. (a) Effect of the incident wavelength on the polymer width (red points) fitted by a Gaussian function (black line). (b) Far-field extinction spectrum of a colloidal AgNP solution in water.

proach is powerful because it provides in a simple manner the near-field spectrum of a single AgNP that has unique information not accessible by far-field measurements. To our knowledge, this is the first time an optical spectrum from a nanostructure has been directly extracted in the near-field. In general, near-field optical spectroscopy is permitted by the use of a tip. However, as pointed out above, what is actually measured in near-field spectroscopy is the far-field signature of the spectrum resulting from the coupling between tip and sample. In the present approach, we used a constant incident normalized dose ($D_0/D_{th}(\lambda)$). The resulting data are dependent mostly on the spectral characteristics of the metal nanoparticle. At the most, the presence of the photopolymer leads to a simple homogeneous spectral shift in accordance with what would be introduced by increasing the surrounding refractive index. In the case of the use of a scanning tip, on the other hand, the spectral dispersion of the particle resonance is expected to depend in a complex manner on the position, nature, and geometry of the tip.

We present for comparison in Figure 8b a far-field ensemble extinction spectrum for a colloidal solution of AgNPs in water. The ensemble far-field spectrum has a plasmon maximum at 452 nm and a broader width that results from inhomogeneous broadening due to NP size dispersion. Using $\Delta\lambda = 4n_m\Delta n_m(d\varepsilon/d\lambda)^{-1}$,[26] where n_m is the refractive index of water, and $\Delta n_m = 1.485 - 1.33 = 0.155$, and based on published values of the silver dielectric function ε,[39] $\Delta\lambda$ was found to be 12 nm for a change in the medium from water to PPF. Thus, the extinction maximum peak of AgNPs is expected at 464 nm. The difference between the far-field spectrum (shifted by 12 nm to account for the refractive index change) and the near-field one is attributed to the size and shape distribution of particles in solution (Figure 2a) and its effects on the inhomogeneous line width of the far-field spectrum.

CONCLUSION

In conclusion, we have presented here a unique approach to quantitatively characterize the near-field of single AgNPs. We demonstrate the ability to directly visualize the optical near-field with sub-10 nm precision by employing photosensitive polymers as molecular probes. Moreover, we were capable of quantifying the near-field depth and enhancement factor as well as measuring a near-field spectrum for an isolated metal nanoparticle. This direct spectral signature allows for interrogation of the near-field spectral response of the AgNPs, which addresses the fundamental difference between near-field and far-field spectra. Furthermore, the localized photopolymerization provides a novel way for fabricating advanced hybrid metal/polymer-based nanophotonic devices. Whereas the interest of the approach is demonstrated here in the well-known case of near-field plasmon dipolar resonance of a spherical Ag nanoparticle, it can be extended to more complex particle geometries that exhibit interesting resonances and various physical phenomena. As an example, we recently showed that this method allows for direct observation of local charge density excitation at the surface of nonresonant metal nanostructures. This study constitutes the subject of an article under preparation. Finally, the method can also be potentially used to probe a larger fraction of the full three-dimensional near-field intensity distribution, whereas previous methods are generally sensitive only to the near-field distribution at the tip apex.

METHODS

Silane Functionalization of the Glass Coverslip. The glass coverslip was functionalized to create an amine-terminated self-assembled monolayer on which silver nanoparticles, stabilized by citrate groups, were strongly bound to the glass surface. This leads to a well-dispersed configuration of commercially synthesized (BBI International) colloidal nanoparticles on the substrate surface.

The overall procedure of the functionalization is described in the following.

Activation of the Substrate. The slide is soaked in a freshly prepared piranha solution (2/3 of H_2SO_4 and 1/3 of H_2O_2) at ambient temperature for 2 h to remove organic impurities and to create silanol groups on the surface followed by thorough rinsing with water.

Silanization of the Slide. The cleaned slide is then submerged in a 0.8% aminosilane solution of anhydrous toluene (<20 ppm of H_2O) for 24 h. Then, the substrate is rinsed with toluene and acetone to remove unbound materials from the surface. This treatment allows us to obtain a monolayer of amine grafted to the surface. This layer is believed to have a thickness of 0.7 nm.[27] Finally, the slide is dried in a stream of dry air. An amine-coated slide is acquired.

Attachment of Silver Nanoparticles to the Slide. The amine-coated substrate is immersed in the silver colloidal solution for 12 h at room temperature to form a monolayer of silver nanoparticles, then rinsed with water and dried with air.

Composition of the Chemical Formulation. The photopolymerizable formulation is made up of three basic components: a sensitizer dye, a co-synergist amine, and a multifunctional acrylate monomer, pentaerythritol triacrylate (PETIA). PETIA was used as received from the supplier and forms the backbone of the polymer network. The co-synergist amine was methyldiethanolamine (MDEA), and the Eosin-Y (2′,4′,5′,7′-tetrabromofluorescein disodium salt) was used as the sensitizer dye. This system was developed mainly because of its high sensitivity in the spectral region from 450 to 550 nm. In addition, this liquid system is very flexible as it is possible to modify the components independently to adjust the physical and the chemical properties of the formulation, namely, viscosity, spectral sensitivity, polymerization threshold, and energy. The results reported in this article were obtained with mixtures containing 0.5 wt % of Eosin-Y and 4 wt % of MDEA.

Acknowledgment. The authors thank the Agence Nationale de la Recherche (ANR), under Grant Photohybrid (BLANC 07-2-188654). P.J. acknowledges UCB Miller Institute funds. L.H. acknowledges the support from the Office of Basic Energy Science of the U.S. Department of the Energy.

Supporting Information Available: Details of the FDTD simulations. This material is available free of charge *via* the Internet at http://pubs.acs.org.

REFERENCES AND NOTES

1. Maier, S. A. *Plasmonics: Fundamental and Applications*; Springer: Berlin, 2007.
2. Zayats, A. V.; Smolyaninov, I. I. Near-Field Photonics: Surface Plasmon Polaritons and Localized Surface Plasmons. *J. Opt. A: Pure Appl. Opt.* **2003**, *5*, 16–50.
3. Deutsch, B.; Hillenbrand, R.; Novotny, L. Visualizing the Optical Interaction Tensor of a Gold Nanoparticle Pair. *Nano Lett.* **2010**, *10*, 652–656.
4. Barnes, W. L.; Dereux, A.; Ebbesen, T. W. Surface Plasmon Subwavelength Optics. *Nature* **2003**, *424*, 824–830.
5. Schuller, J. A.; Barnard, E. S.; Cai, W.; Jun, Y. C.; White, J. S.; Brongersma, M. L. Plasmonics for Extreme Light Concentration and Manipulation. *Nat. Mater.* **2010**, *9*, 193–204.
6. Atwater, H. A.; Polman, A. Plasmonics for Improved Photovoltaic Devices. *Nat. Mater.* **2010**, *9*, 205–213.
7. Kamat, P. V.; Schatz, G. C. Nanotechnology for Next Generation Solar Cells. *J. Phys. Chem. C* **2009**, *113*, 15473–15475.
8. Cole, J.; Halas, N. J. Optimized Distributions of Tunable Plasmonic Nanoparticles for Solar Light Harvesting Applications. *Appl. Phys. Lett.* **2006**, *89*, 153120.
9. Juan, M. L.; Gordon, R.; Pang, Y.; Eftekhari, F.; Quidant, R. Self-Induced Back-Action Optical Trapping of Dielectric Nanoparticles. *Nat. Phys.* **2009**, *5*, 915–919.
10. Noginov, M. A.; Zhu, G.; Belgrave, A. M.; Bakker, R.; Shalaev, V. M.; Narimanov, E. E.; Stout, S.; Herz, E.; Suteewong, T.; Wiesner, U. Demonstration of a Spaser-Based Nanolaser. *Nature* **2009**, *460*, 1110–1112.
11. Bergman, D. J.; Stockman, M. I. Surface Plasmon Amplification by Stimulated Emission of Radiation: Quantum Generation of Coherent Surface Plasmons in Nanosystems. *Phys. Rev. Lett.* **2003**, *90*, 027402–027405.
12. Eghlidi, H.; Lee, K. G.; Chen., X. W.; Götzinger, S.; Sandoghdar, V. Resolution and Enhancement in Nanoantenna-Based Fluorescence Microscopy. *Nano Lett.* **2009**, *9*, 4007–4011.
13. Baffou, G.; Quidant, R.; Garcia de Abajo, F. J. Nanoscale Control of Optical Heating in Complex Plasmonic Systems. *ACS Nano* **2010**, *4*, 709–716.
14. Cole, J. R.; Mirin, N. A.; Knight, M. W.; Goodrich, G. P.; Halas, N. J. Photothermal Efficiencies of Nanoshells and Nanorods for Clinical Therapeutic Applications. *J. Phys. Chem. C* **2009**, *113*, 12090–12094.
15. Haes, A. W.; Hall, W. P.; Chang, L.; Klein, W. L.; Van Duyne, R. P. A Localized Surface Plasmon Resonance Biosensor: First Steps toward an Assay for Alzheimer's Disease. *Nano Lett.* **2004**, *4*, 1029–1034.
16. El-Sayed, I. H.; Huang, X.; El-Sayed, M. A. Surface Plasmon Resonance Scattering and Absorption of Anti-EGFR Antibody Conjugated Gold Nanoparticles in Cancer Diagnostics: Applications in Oral Cancer. *Nano Lett.* **2005**, *5*, 829–834.
17. Hubert, C.; Rumyantseva, A.; Lerondel, G.; Grand, J.; Kostcheev, S.; Billot, L.; Vial, A.; Bachelot, R.; Royer, P.; Chang, S. H.; *et al.* Near-field Photochemical Imaging of Noble Metal Nanostructures. *Nano Lett.* **2005**, *5*, 615–619.
18. Srituravanich, W.; Pan, L.; Wang, Y.; Sun, C.; Bogy, D. B.; Zhanget, X. Flying Plasmonic Lens in the Near Field for High-Speed Nanolithography. *Nat. Nanotechnol.* **2008**, *3*, 733–737.
19. Anker, J. N.; Hall, W. P.; Lyandres, O.; Shah, N. C.; Zhao, J.; Van Duyne, R. P. Biosensing with Plasmonic Nanosensors. *Nat. Mater.* **2008**, *7*, 442–453.
20. Alivisatos, P. The Use of Nanocrystals in Biological Detection. *Nat. Biotechnol.* **2004**, *22*, 47–52.
21. Wiederrecht, G. P. Near-Field Optical imaging of Noble Metal Nanoparticles. *Eur. Phys. J. Appl. Phys.* **2004**, *28*, 3–18.
22. Bouhelier, A. Field-Enhanced Scanning Near-Field Optical Microscopy. *Microsc. Res. Tech.* **2006**, *69*, 563–579.
23. Nelayah, J.; Kociak, M.; Stephan, O.; Garcia de Abajo, F. J.; Tence, M.; Henrard, L.; Taverna, D.; Pastoriza-Santos, I.; Liz-Marzan, L. M.; Colliex, C. Mapping Surface Plasmons on a Single Metal Nanoparticle. *Nat. Phys.* **2008**, *3*, 348–353.
24. Douillard, L.; Charra, F.; Korczak, Z.; Bachelot, R.; Kostcheev, S.; Lerondel, G.; Adam, P. M.; Royer, P. Short Range Plasmon Resonators Probed by Photoemission Electron Microscopy. *Nano Lett.* **2008**, *8*, 935–940.
25. Hohenester, U.; Ditlbacher, H.; Krenn, J. R. Electron-Energy-Loss Spectra of Plasmonic Nanoparticles. *Phys. Rev. Lett.* **2009**, *103*, 106801–106804.
26. Ibn El Ahrach, H.; Bachelot, R.; Vial, A.; Lerondel, G.; Plain, J.; Royer, P.; Soppera, O. Spectral Degeneracy Breaking of the Plasmon Resonance of Single Metal Nanoparticles by Nanoscale Near-Field Photo-Polymerization. *Phys. Rev. Lett.* **2007**, *98*, 107402–107405.
27. Plain, J.; Sonnefraud, Y.; Viste, P.; Lerondel, G.; Huant, S; Royer, P. Self-Assembly Drives Quantum Dot Photoluminescence. *J. Fluoresc.* **2003**, *19*, 311–316.
28. Ecoffet, C.; Espanet, A.; Lougnot, D. J. Photopolymerization by Evanescent Waves: A New Method To Obtain Nanoparts. *Adv. Mater.* **1998**, *10*, 411–414.
29. Wurtz, G.; Bachelot, R.; H'Dhili, F.; Royer, P.; Triger, C.; Ecoffet, C.; Lougnot, D. J. Photopolymerization Induced by Optical Field Enhancement in the Vicinity of a Conducting Tip under Laser Illumination. *Jpn. J. Appl. Phys.* **2000**, *39*, 98–100.
30. Srituravanich, W.; Fang, N.; Sun, C.; Luo, Q.; Zhang, X. Plasmonic Nanolithography. *Nano Lett.* **2004**, *4*, 1085–1088.
31. Sundaramurthy, A.; Schuck, P. J.; Conley, N. R.; Fromm, D. P.; Kino, G. S.; Moerner, W. E. Toward Nanometer-Scale Optical Photolithography: Utilizing the Near-Field of Bowtie Optical Nanoantennas. *Nano Lett.* **2006**, *6*, 355–360.
32. Ueno, K.; Takabatake, S.; Nishijima, Y.; Mizeikis, V.; Yokota, Y.; Misawa, H. Nanogap-Assisted Surface Plasmon Nanolithography. *J. Phys. Chem. Lett.* **2010**, *1*, 657–662.
33. Orfanidis, S. J. Electromagnetic Waves and Antennas; http://www.ece.rutgers.edu/orfanidi/ewa/, 2008.
34. Goodman, J. W. *Introduction to Fourier Optics*; McGraw-Hill Science: New York, 1996.
35. Jain, P. K.; Huang, W.; El-Sayed, M., A. On the Universal Scaling Behavior of the Distance Decay of Plasmon Coupling in Metal Nanoparticle Pairs: A Plasmon Ruler Equation. *Nano Lett.* **2007**, *7*, 2080–2088.
36. Aubert, S.; Bruyant, A.; Blaize, S.; Bachelot, R.; Lerondel, G.; Hudlet, S.; Royer, P. Analysis of the Interferometric Effect of the Background Light in Apertureless Scanning Near-Field Optical Microscopy. *J. Opt. Soc. Am. B: Opt. Phys.* **2003**, *20*, 2117–2124.
37. Sandoghdar, V.; Mlynek, J. Prospects in Apertureless SNOM with Active Probes. *J. Opt. A: Pure Appl. Opt.* **1999**, *1*, 523–530.
38. Wang, H.; Wu, Y.; Lassiter, B.; Nehl, C. L.; Hafner, J. H.; Nordlander, P.; Halas, N. J. Symmetry Breaking in Individual Plasmonic Nanoparticles. *Proc. Natl. Acad. Sci. U.S.A.* **2006**, *103*, 10856–10860.
39. Palik, E. D. *Handbook of Optical Constants of Solids*; Academic Press: Orlando, FL, 1985.